Ultrasound in Med. & Biol., Vol. 00, No. 00, pp. 1–12, 2021

0301-5629/$ - see front matter

https://doi.org/10.1016/j.ultrasmedbio.2021.08.004

● *Original Contribution*

HISTOTRIPSY ABLATION OF BONE TUMORS: FEASIBILITY STUDY IN EXCISED CANINE OSTEOSARCOMA TUMORS

Lauren Arnold,* Alissa Hendricks-Wenger,*,†,‡ Sheryl Coutermarsh-Ott,† Jessica Gannon,*,§ Alayna N. Hay,¶ Nikolaos Dervisis,¶,‖,# Shawna Klahn,¶ Irving C. Allen,†,‡,‖ Joanne Tuohy,¶ and Eli Vlaisavljevich*,‖

* Department of Biomedical Engineering and Mechanics, Virginia Tech, Blacksburg, Virginia, USA; † Department of Biomedical Sciences and Pathobiology, Virginia–Maryland College of Veterinary Medicine, Blacksburg, Virginia, USA; ‡ Graduate Program in Translational Biology, Medicine and Health, Virginia Tech, Roanoke, Virginia, USA; § Department of Mechanical Engineering, Virginia Tech, Blacksburg, Virginia, USA; ¶ Department of Small Animal Clinical Sciences, Virginia–Maryland Regional College of Veterinary Medicine, Blacksburg, Virginia, USA; ‖ ICTAS Center for Engineered Health, Virginia Tech, Kelly Hall, Blacksburg, Virginia, USA; and # Department of Internal Medicine, Virginia Tech Carilion School of Medicine, Roanoke, Virginia, USA

(*Received* 28 *April* 2021; *revised* 27 *July* 2021; *in final form* 4 *August* 2021)

Abstract—Osteosarcoma (OS) is a primary bone tumor affecting both dogs and humans. Histotripsy is a non-thermal, non-invasive focused ultrasound method using controlled acoustic cavitation to mechanically disintegrate tissue. In this study, we investigated the feasibility of treating primary OS tumors with histotripsy using a 500-kHz transducer on excised canine OS samples harvested after surgery at the Veterinary Teaching Hospital at Virginia Tech. Samples were embedded in gelatin tissue phantoms and treated with the 500-kHz histotripsy system using one- or two-cycle pulses at a pulse repetition frequency of 250 Hz and a dosage of 4000 pulses/point. Separate experiments also assessed histotripsy effects on normal canine bone and nerve using the same pulsing parameters. After treatment, histopathological evaluation of the samples was completed. To determine the feasibility of treating OS through intact skin/soft tissue, additional histotripsy experiments assessed OS with overlying tissues. Generation of bubble clouds was achieved at the focus in all tumor samples at peak negative pressures of 26.2 ± 4.5 MPa. Histopathology revealed effective cell ablation in treated areas for OS tumors, with no evidence of cell death or tissue damage in normal tissues. Treatment through tissue/skin resulted in generation of well-confined bubble clouds and ablation zones inside OS tumors. Results illustrate the feasibility of treating OS tumors with histotripsy. (E-mail: EliV@vt.edu)

Key Words: **Histotripsy, Focused ultrasound, Osteosarcoma, Bone, Tumors, Ablation.**

INTRODUCTION

Osteosarcoma (OS) is the most common primary malignant bone tumor in both humans and dogs. In both species, appendicular OS is predominant, occurring most frequently in the metaphysis of long bones; less often, OS affects the axial skeleton (Longhi et al. 2006; Morello et al. 2011; Fenger et al. 2014). OS has an incidence of ~1/100,000 in humans across all ages, with an increased incidence of up to 11/100,000 in the age group 15–19 y (Brodey 1979; Fenger et al. 2014; Luetke et al. 2014). The 5-year survival rate in humans with non-metastatic OS is 60%–70%, with an estimated 20%–30% long-term survival in patients with identifiable metastases at diagnosis (Friebele et al. 2015; Meazza and Scanagatta 2016). OS occurs about 10 times more often in dogs than humans, with an incidence of 13.9/100,000 and a 1-y survival rate of only ~45% with definitive treatment (Rowell et al. 2011; Simpson et al. 2017).

The current standard of care for human patients with OS includes pre- and post-operative chemotherapy and surgical removal of primary and metastatic lesions. Historically, amputation has been the primary surgical approach to appendicular OS, but therapeutic advances have increased limb-salvage procedures, making limb salvage a viable alternative in 80%–85% of human OS cases (Wafa and Grimer 2006). Despite these advances, 80%–90% of patients are estimated to have micrometastases present at initial diagnosis, and 30%–40% of

Address correspondence to: Eli Vlaisavljevich 347 Kelly Hall, 325 Stanger Street, Blacksburg, VA 24061, USA. E-mail: EliV@vt.edu

patients with localized OS will develop a local or distant recurrence (Luetke et al. 2014). New chemotherapy regimens have also failed to increase median survival time, and alternative treatments such as immunotherapy remain experimental (Luetke et al. 2014). In dogs, OS treatments closely resemble those of humans, with surgical resection of the primary tumor via limb amputation or limb-salvage surgery being the standard treatment along with adjuvant chemotherapy to control the risk for metastatic disease (LeBlanc et al. 2021). Unlike in humans, amputations remain the primary surgical option compared with limb-salvage surgeries because of the high rate of complications in canine limb-salvage surgeries, including infection, implant failure and tumor recurrence (Szewcyzk et al. 2015; Mitchell et al. 2016). Together, these limitations indicate a significant need for improved, non-surgical treatment options that preserve limb function with fewer complications (Szewcyzk et al. 2015). Additional limitations to current OS therapies for both humans and dogs include low responsivity to chemotherapy in some patients and an inability to surgically remove some tumors with sufficient margins to prevent local recurrence.

Ablation methods have been investigated as minimally invasive treatments for primary and metastatic bone tumors (Callstrom et al. 2006; Ward et al. 2008; Callstrom and Kurup 2009; Ding et al. 2009; Jones et al. 2010; Errani et al. 2011). Ablation is used primarily as a palliative treatment in patients who are unable to tolerate a major surgical procedure because of comorbidities or the presence of multiple metastatic lesions. Several different technologies have been investigated for the local ablation of tissue with thermal techniques, including radiofrequency ablation, microwave ablation, cryoablation and laser ablation (Errani et al. 2011). These thermal therapies have had some success for pain mediation in patients with primary bone tumors and metastases (Callstrom et al. 2006; Errani et al. 2011). However, they remain limited in ablative efficiency near neurovascular structures or skin because of the risk of nerve, vascular or skin damage (Errani et al. 2011). Additionally, these therapies may be subject to the heat sink effect originating from blood flow, which can result in incomplete tumor necrosis in regions near major vessels (Patterson et al. 1998; Curley 2001; Zachos et al. 2001; Lu et al. 2003; Marrero and Pelletier 2006). The heat sink effect can be especially problematic in bone tumors with a large soft tissue component. There are also limitations with tumor size using these techniques, with tumors >3 cm requiring an unsuitably long treatment time (Patterson et al. 1998; Curley 2001; Lu et al. 2003; Marrero and Pelletier 2006). High-intensity focused ultrasound (HIFU) is a non-invasive thermal technique that has also been investigated for the treatment of bone tumors, with results of similar responses for pain mediation (Li et al. 2009; Chen et al. 2010; Li et al. 2010; Napoli et al. 2013; Yu et al. 2015). HIFU represents an improvement on other thermal ablation methods because of its non-invasive nature and ability to target tumors in locations not accessible to percutaneous approaches. However, like other thermal ablation methods, HIFU presents the risk of damaging neurovascular tissues and may cause burns when used directly under the skin. For all these reasons, there remains a critical need for alternative OS treatments that overcome the limitations of ablation and the current standard of care.

Histotripsy is a non-thermal, non-invasive focused ultrasound method that uses highly controlled, high-amplitude ultrasound pulses to generate acoustic cavitation (*i.e.,* bubble cloud), mechanically disintegrating tissue into subcellular components with high precision (millimeter accuracy) (Xu et al. 2004; Parsons et al. 2005; Roberts et al. 2006; Lin et al. 2014; Vlaisavljevich et al. 2016a, 2016b; Bader et al. 2019). Unlike ablation using thermal techniques, previous studies have established that histotripsy does not induce significant temperature changes on overlying tissues or at the treatment focus, permitting the ablation of target tissues without inducing thermal damage to adjacent healthy tissues (Kim et al. 2014a, 2014b). While prior work has established the potential of histotripsy to achieve complete ablation of many soft tissues, studies have also found that tissue properties affect the susceptibility of a tissue to histotripsy damage, with tissues of increased mechanical strength and density (*e.g.,* cartilage, tendon, bone, large vascular structures) exhibiting decreased or no ablation after treatment (Lake et al. 2008a, 2008b; Vlaisavljevich et al. 2014, 2015a, 2015b). Because of these differences in tissue susceptibility, histotripsy provides increased potential for preservation of adjacent critical structures such as blood vessels, nerves and ducts (Lake et al. 2008a, 2008b; Vlaisavljevich et al. 2013, 2014a, 2014b, Smolock et al. 2018). The differences in tissue susceptibility, however, may also make it difficult to treat OS tumors, which may have tissue properties (*e.g.,* stiffness, mechanical strength) closer to those of cartilage and bone than to soft tissues. Another benefit of histotripsy is that the cavitation bubble cloud and the resulting tissue ablation are clearly visible on ultrasound imaging and magnetic resonance imaging, permitting real-time monitoring of treatment delivery and tissue disintegration (Vlaisavljevich et al. 2013; Allen et al. 2014, Allen et al., 2017; Smolock et al. 2018; Bader et al. 2019). These features have made histotripsy a promising new therapy for multiple applications, including a recent clinical trial for the treatment of liver cancer (Vidal Jove et al. 2019). However, there have been no studies to date that investigate

the feasibility of using histotripsy for the treatment of OS tumors.

The objective of this study was to determine the feasibility of ablating primary OS tumors with histotripsy using *ex vivo* canine OS tumor samples and a 500-kHz histotripsy system. Tumor samples included sectioned tumor samples embedded in gelatin tissue phantoms and whole-tumor samples containing intact overlying skin/tissue. Separate experiments were also conducted to assess the effects of histotripsy on normal canine bone and nerve to assess whether these structures could be preserved during OS histotripsy treatment.

METHODS

Histotripsy system

A custom 32-element 500-kHz histotripsy transducer was used to assess the feasibility of using in ablation of excised canine osteosarcomas. The 500-kHz frequency, which is towards the lower end of the frequency range that has been explored for histotripsy treatments in prior studies (~250 kHz−2 MHz), was selected based on prior studies suggesting that lower frequency may enhance the ablative efficacy of histotripsy in stiffer tissues (such as OS tumors) because it enhances bubble expansion while also reducing the total treatment time required for volumetric ablation caused by the larger bubble clouds (Vlaisavljevich et al. 2015a, 2015b). For the first part of this work, the array transducer was configured as three concentric circles of 6, 12 and 14 piezoelectric elements 20 mm in diameter with a geometric focus of 75 mm, an aperture size of 120.5 mm and an *f*-number of 0.62 (Fig. 1a). The transducer was driven using a custom high-voltage pulser designed to generate short therapy pulses of <2 cycles. The high-voltage pulser was controlled by a field-programmable gate array board (Altera DE0-Nano Terasic Technology, Dover, DE, USA) programmed for histotripsy therapy pulsing. The transducer was positioned horizontally in a tank of degassed water (<30% dissolved O_2), and a computer-guided 3-D positioning system was used to orient the gelatin tissue phantoms containing the tissue samples (Fig. 2a). A linear ultrasound imaging probe with a frequency range of 5−18 MHz (SL18-5, SuperSonic Imagine, Aix-en-Provence, France) was perpendicularly aligned with the geometric focus of the transducer for real-time treatment guidance and monitoring. MATLAB (The MathWorks, Natick, MA, USA) controlled the positioning system and the transducer simultaneously to guide the automated volumetric tissue treatments, and the transducer was powered by a high-voltage DC power supply (PLH120-P, Aim-TTi, Cambridgeshire, UK). The histotripsy array transducer was used in this configuration to treat the six OS samples in the first part of this work and the normal bone and nerve samples.

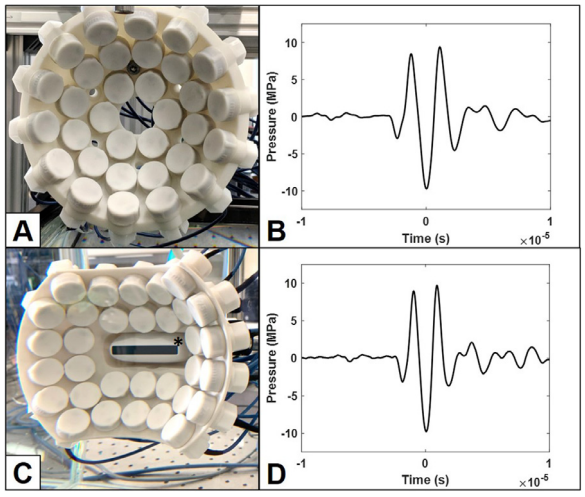

Fig. 1. Histotripsy transducer configurations and representative pressure waveforms at a *p*- ~10 MPa. Configuration 1 (a, b) was used to assess the feasibility of treating osteosarcoma with histotripsy. Configuration 2 (c, d) was designed to test a clinically relevant histotripsy setup with coaxial US imaging guidance (*asterisk*).

In the second part of this work, the 32-element 500-kHz transducer was modified into a more clinically relevant transducer configuration. A separate transducer scaffold was designed to allow for coaxial ultrasound imaging while closely mimicking the parameters of the original configuration. The new transducer scaffold was designed to fit two rectangular rings of 14 and 18 piezoelectric elements 20 mm in diameter positioned around a central hole in the therapy transducer sized to fit a coaxially aligned linear ultrasound imaging probe. The scaffold was populated with the same set of 32 piezoelectric elements from the first part of this study and used the same linear ultrasound probe for treatment guidance and monitoring (Fig. 1c). The clinical transducer configuration had a geometric focus of 78 mm, an elevational aperture size of 112 mm and a transverse aperture size of 128 mm, with *f*-numbers of 0.70 (elevational) and 0.61 (transverse). This modified configuration was used for the final histotripsy ablation experiments in two OS samples containing skin and overlying tissues to better replicate the expected experimental setup for future i*n vivo* studies. The modified transducer was driven using the same parameters and components as the transducer in its original configuration.

Hydrophone focal pressure measurements and beam profiles

Focal pressure waveforms for the 500-kHz transducer were measured using a custom-built fiberoptic hydrophone (FOPH) in degassed water at the focal point of each transducer (, 2006). The FOPH was cross-

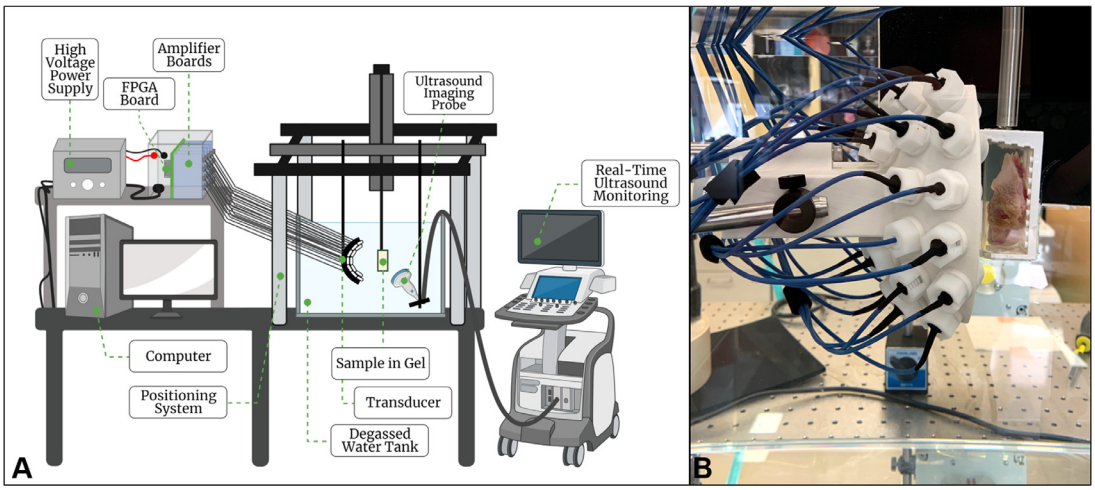

Fig. 2. Experimental histotripsy. A 500-kHz histotripsy transducer was used to treat all samples in one of two configurations, with real-time ultrasound imaging (either perpendicular [configuration 1] or coaxial [configuration 2]) used to capture cavitation behavior inside of excised canine osteosarcoma samples fixed in gelatin. FPGA = field-programmable gate array. Figure 2a was created with Biorender.com.

calibrated at low pressure values with a high-sensitivity reference rod hydrophone (HNR-0500, Onda Corp., Sunnyvale, CA, USA) to ensure accurate pressure measurements were collected with the FOPH. The rod hydrophone was also used to measure the focal beam profiles of the transducer in both configurations. The lateral, elevational and axial 1-D beam profiles of each transducer were measured by scanning the hydrophone incrementally over a distance wider than the focal width at a peak negative pressure (p-) of ~1.8 MPa. For the original configuration, the transverse, elevational and axial full-width half-maximum dimensions at the geometric focus of the transducer were measured to be 2.2, 2.2 and 6.5 mm, respectively (Edsall et al. 2021). The modified configuration had beam dimensions only slightly different from those of the original, with the transverse, elevational and axial full-width half-maximum dimensions at the focus measured to be 2.1, 2.1 and 6.6 mm. All reported focal pressures were directly measured with the FOPH in degassed water in free field up to a p_- of ~20 MPa. At p- greater than ~20 MPa, p-values could not be measured directly because cavitation was stabilized at the tip of the FOPH fiber, and the focal pressure was measured instead by summing measurements from subsets of 8 and 16 elements (Vlaisavljevich et al., 2017a). All waveforms were measured using a Tektronix TBS2000 series oscilloscope at a sample rate of 500 MS/s; then, the waveform data were averaged over 512 pulses and recorded in MATLAB.

Tissue specimens for excised tissue treatments

Excised canine OS samples were obtained after standard-of-care limb amputation from patients with appendicular OS at the Virginia−Maryland Veterinary Teaching Hospital (Blacksburg, VA, USA) in accordance with the Virginia Tech Institutional Animal Care and Use Committee under IACUC Approval No. 19-162. After surgery, the amputated limbs were sent to the pathology laboratory, where samples of the tumor were collected for histopathological analysis. Any tissue not needed for histopathological evaluation was donated to this study. After sterile harvesting, the OS samples were placed in Dulbecco's Modified Eagle's Medium (DMEM) (Low-Glucose DMEM, No. 31600034, Thermo Fisher Scientific, Waltham, MA, USA) and transferred to the histotripsy team to be prepared for treatment. Before treatment, samples were placed inside of a saline solution in a vacuum chamber (60−85 kPa) for a minimum of 2 h to remove any gas introduced within the tissue during storage/transport (Vlaisavljevich et al. 2015a, 2015b). After degassing, the OS samples were embedded in 7.5% gelatin in degassed saline (gelatin from porcine skin, Sigma-Aldrich, St. Louis, MO, USA) tissue phantoms for treatment. Gel phantoms containing the embedded tumor samples were then refrigerated to solidify the gel. Normal canine bone and nerve samples from portions of the amputated limbs appropriately distant to the tumor were also collected by the veterinary team to assess whether histotripsy could spare critical structures inside of or immediately adjacent to malignant tumor tissue. Normal, non-neoplastic bone samples and a sciatic nerve sample ~0.5 cm in diameter were used. After harvesting, the healthy canine bone and nerve samples were prepared for treatment using the same procedures as the OS tissues. All samples were treated within 48 h of harvest and

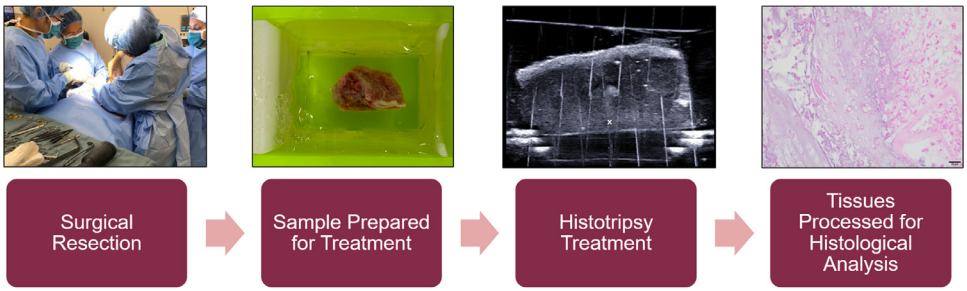

Fig. 3. Experimental workflow for excised canine osteosarcoma tumor histotripsy treatment and analysis. Osteosarcoma samples were harvested after standard-of-care limb amputation, fixed in gelatin for treatment, treated with a 500-kHz histotripsy transducer using 1- or 2-cycle pulses at a dosage of 4000 pulses per point and histologically analyzed after treatment.

within 24 h of phantom preparation. Figure 3 summarizes the experimental workflow for the OS histotripsy experiments.

Histotripsy ablation of ex vivo *OS tumors*

The feasibility of treating canine OS using histotripsy was investigated by subjecting the excised tissue samples embedded inside gelatin phantoms to histotripsy. For all experiments, the 500-kHz histotripsy transducer was used to apply 1- or 2-cycle histotripsy pulses to the center of the OS samples at a pulse repetition frequency (PRF) of 250 Hz. During each treatment, OS samples fixed in gelatin were mounted to a motorized 3-D positioning system and aligned to the focus of the therapy transducer (Fig. 1a). The treatments were guided by an ultrasound imaging probe (SL18-5, SuperSonic Imagine) used to visualize the histotripsy cavitation bubble cloud in real time throughout histotripsy treatment. Six excised OS samples were treated with the histotripsy transducer in its original configuration with the ultrasound imaging mounted perpendicularly to the tissue and aligned to the focal location of the therapy transducer. Before the embedded OS samples were positioned, the geometric focus of the histotripsy transducer was located and marked on the imaging screen by generating a bubble cloud in open water and then marking the location of the cloud on the imaging screen. Next, the embedded OS sample was aligned to the focus by positioning the marked focal point at the desired location within the OS tissue. The pressure required to generate histotripsy cavitation inside of each sample was measured by gradually increasing the pressure at the focus until a consistent histotripsy bubble cloud was identified on real-time US imaging (Vlaisavljevich et al. 2013; Smolock et al. 2018). This pressure level was recorded as the cavitation cloud threshold for each sample.

After identification of the cavitation cloud threshold for each sample, experiments were conducted to determine the feasibility of using histotripsy to ablate a targeted tissue volume in each OS sample. A target volume was chosen for each sample based on the sample's size and orientation compared with the experimentally calculated size of the histotripsy bubble cloud. When possible, the portion of the OS sample containing primarily tumor and lytic regions was targeted for histotripsy treatment (*i.e.,* regions containing fully intact bone were avoided) to provide more consistent and relevant results between samples. Targeted volumes ranged from 27 mm^3 ($3 \times 3 \times 3$ mm) to 125 mm^3 ($5 \times 5 \times 5$ mm). Histotripsy was then applied to the targeted volume at a pressure level ~20% above the cavitation threshold. For these experiments, the applied p- ranged between 24 and 37 MPa depending on the sample being treated. Automated volumetric treatments were then applied to a predetermined 3-D grid of equidistant treatment points. Treatment points were spaced by 2.5 mm in the axial direction and 1 mm in the lateral directions to allow overlap between the bubble clouds at each location. Each treatment point within the programmed grid was uniformly treated with histotripsy by mechanically scanning the therapy focal zone through the targeted volume of the OS sample, with 4000 histotripsy pulses applied to each point targeted. This relatively high treatment dose was chosen for the feasibility study based on previous work investigating histotripsy for the ablation of different tissue types, in which it was found that stiffer tissues require higher treatment dosages for cell lysis to occur, and on the hypothesis that OS tumors may be less susceptible to histotripsy because of their composition (Rho et al. 1993; Vlaisavljevich et al. 2014a, 2014b).

Hydrophone focal pressure measurements and beam profiles

Healthy canine bone and nerve samples were treated using the same experimental histotripsy setup as detailed above. In short, healthy canine bone and nerve samples embedded in gelatin were mounted to a 3-D positioning system and aligned to the focus of the

therapy transducer. The 500-kHz histotripsy transducer was used to apply 1- or 2-cycle histotripsy pulses to the center of the samples at a PRF of 250 Hz. The focal location was identified and marked by firing histotripsy pulses in open water, and the sample was aligned to this location. The pressure required to generate a histotripsy bubble cloud inside of each sample was determined by incrementally increasing the pressure at the focus until consistent cavitation was observed on US imaging. Targeted regions were again chosen based on the sample's size to contain the ablation zone within the sample. The samples were treated at a pressure ~20% above the cavitation threshold at 4000 pulses/point at each treatment location. For these experiments, the applied *p*- ranged from 13−16 MPa depending on the sample. Treatment pressures lower relative to those used for the OS sample treatments were chosen because of the lower cavitation threshold observed in these samples and the high prevalence of prefocal cavitation at the tissue boundary. When treatment pressures were increased to the level of the OS treatments, the prefocal cavitation overwhelmed the focal histotripsy bubble cloud, and precise, focal cavitation was lost. Automated volumetric treatments were performed by scanning the focus of the therapy transducer through a 3-D grid of treatment points spaced as described earlier. For all experiments, real-time US imaging was used to visualize the histotripsy bubble cloud inside the tissue sample throughout the entire treatment

Feasibility of clinical histotripsy OS ablation

To assess image-guided histotripsy treatments of canine OS through clinically relevant overlying tissues, two additional excised canine OS samples with intact overlying skin and muscle tissues were treated with histotripsy according to the procedures outlined above. In short, the transducer configuration was modified to permit the use of coaxial imaging, and the modified 500-kHz histotripsy transducer was used to apply 1- or 2-cycle histotripsy pulses to the center of the OS samples at a PRF of 250 Hz. A coaxially aligned ultrasound imaging probe (SL18-5, SuperSonic Imagine) was used to visualize the histotripsy cavitation bubble cloud in real time throughout histotripsy treatment. Then, the location of the transducer bubble cloud was identified, the embedded OS sample was aligned to the transducer focus and the cavitation cloud threshold for each sample was identified. After recording the cavitation cloud threshold for each sample, a target volume was chosen based on each sample's size and orientation. Targeted volumes for these two samples were 432 mm^3 (6 × 6 × 12 mm) and 480 mm^3 (7.5 × 8 × 8 mm), respectively. Through application of histotripsy at a pressure level ~20% greater than the tissue's cavitation threshold, a volumetric treatment of each sample was completed, with 4000 histotripsy pulses applied per treatment point. Peak negative pressures used for these two treatments were 29 and 33 MPa, respectively.

Histological and morphological analysis

After treatment, tissue specimens were visually inspected and fixed in 10% formalin for a minimum of 24 h post-treatment before sectioning and staining. A standard hematoxylin and eosin (H&E) stain was used to stain all tissues to assess the extent of histotripsy damage to the tissue. Changes in the structure and density of collagen and other tissue structures were noted within the ablation volume. To determine the estimated percentage of tissue ablated within the targeted volume, individuals trained by a veterinary pathologist compared regions of cellular damage with regions outside of the ablation zone. Results were verified by a board-certified veterinary pathologist (S.C.O.) to ensure accuracy.

RESULTS

Histotripsy ablation of ex vivo *OS specimens*

The ability of histotripsy to ablate OS tumors was assessed using canine tumor samples collected after amputation, as described under Methods. Excised OS tumor samples (Fig. 4a) varied in composition, with heterogeneity present within individual samples and notable differences observed between different samples histologically. For instance, some samples contained large regions of bone or mineralized tissue minimally affected by the tumor and with good structural integrity interspersed with smaller regions of lytic, tumor-ridden bone. Other samples were composed of softer, lytic bone and soft tissue tumor components with little to no intact bone. The *p*- required to generate histotripsy bubble clouds inside of the excised OS samples ranged from 20.3−31.3 MPa, with the average cavitation cloud pressure threshold measured to be 25.5 ± 4.2 MPa. On ultrasound imaging, the bubble clouds in all excised tissues were clearly visible within the focal region of the transducer (Fig. 4b). Histotripsy bubble clouds were observed on ultrasound imaging as dense, dynamically changing hyperechoic regions and were maintained throughout the length of treatment in all tissue experiments. In some samples, occasional cavitation events were observed prefocally within the tissue sample or at the gelatin−tissue interface. Histological staining of non-treated OS tumors revealed variably dense populations of neoplastic cells, occasionally effacing cortical bone (Fig. 4b, 4c). In these non-treated samples, tumor cells were readily identified, with light pink osteoid matrix present within the samples

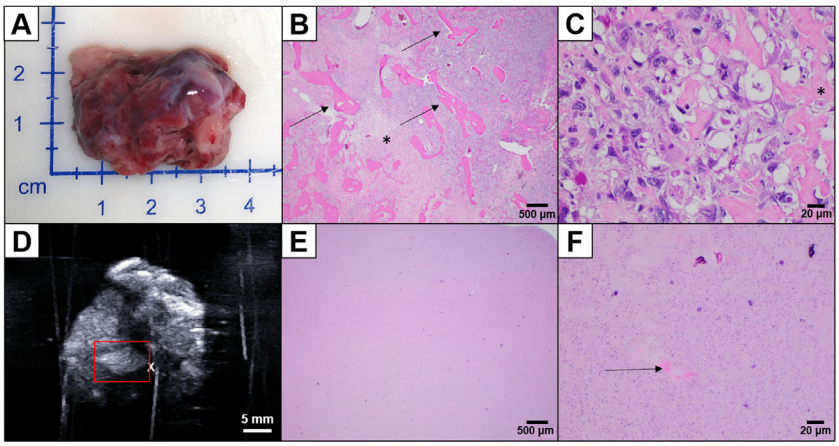

Fig. 4. Representative histotripsy treatment of a canine osteosarcoma sample without overlying tissue. (a) Excised canine osteosarcoma before histotripsy treatment. (b) Untreated tumor tissue (magnification: 2 ×) is often characterized by sheets of neoplastic cells (*asterisk*) effacing cortical bone (*arrows*). (c) Untreated tumor tissue (magnification: 40 ×). Neoplastic cells variably produce tumor bone termed *osteoid* (*asterisk*). (d) Visualization of the histotripsy bubble cloud (*boxed*) during treatment. (e) Treated tumor tissue (magnification: 2 ×) was typically characterized by complete loss of recognizable architecture with only faintly basophilic, stippled debris remaining. (f) Treated tumor tissue (magnification: 40 ×) exhibits basophilic debris and occasional remnants of osteoid (*arrow*).

(Fig. 4b, 4c). After histotripsy treatment, a complete loss of tissue architecture and cellular detail was observed. Cellular debris was observed in histological staining, with a few rare foci of light pink osteoid, but reduced in size compared with the untreated samples (Fig. 4e, 4f). These results were consistent across samples, with rare remaining cell nuclei present in some treated tissues but no intact tumor cells remaining within the treated volume of any of the histotripsy-treated samples. No signs of thermal injury were observed in any of the treated samples.

Histotripsy ablation of healthy critical structure samples

To assess whether histotripsy could spare critical structures inside of or immediately adjacent to malignant tumor tissue, normal canine bone and nerve samples were treated using the custom histotripsy transducer, as described under Methods. Two healthy canine bone samples were tested, with *p*- of 11.8 and 13.5 MPa required to generate histotripsy bubble clouds inside of the tissue samples. One healthy canine sciatic nerve sample was tested. A *p*- of 10.7 MPa was required to generate a histotripsy bubble cloud in this sample. In all samples, bubble clouds were clearly visible on ultrasound as dense, dynamically changing hyperechoic regions. Two healthy canine bone samples and one healthy canine sciatic nerve sample were treated with histotripsy in this study at treatment parameters equivalent to those used in the OS histotripsy treatments (4000 pulses/point). In Figure 5 are representative images of untreated (Fig. 5a, 5b) and treated (Fig. 5c, 5d) canine cortical bone tissues. There were no histologic differences between the treated and untreated cortical bone samples. In Figure 6 are representative images of untreated (Fig. 6a, 6b) and treated (Fig. 6c, 6d) healthy canine sciatic nerve samples. Again, no histologic differences were observed between the treated and untreated sciatic nerve samples.

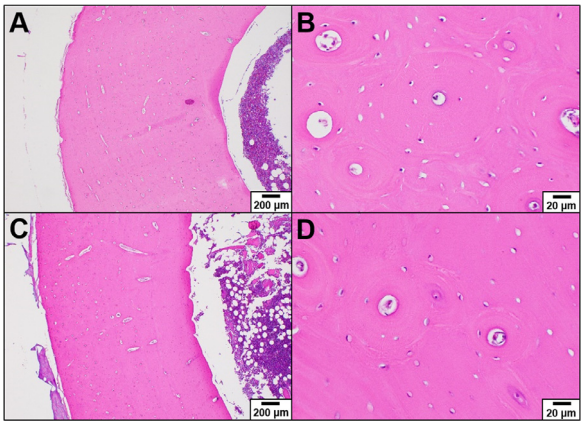

Fig. 5. Normal, healthy neoplastic bone was excised from amputated canine limbs and subjected to histotripsy. No histological differences were noted between untreated samples (a: magnification 4 ×, b: magnification 40 ×) and treated samples (c: magnification 4 ×, d: magnification 40 ×).

Clinically relevant histotripsy ablation of ex vivo *osteosarcoma*

Two amputated limbs with OS tumors and intact overlying intact tissue were treated to test histotripsy ablation of OS in a clinically relevant configuration using coaxially aligned ultrasound image guidance.

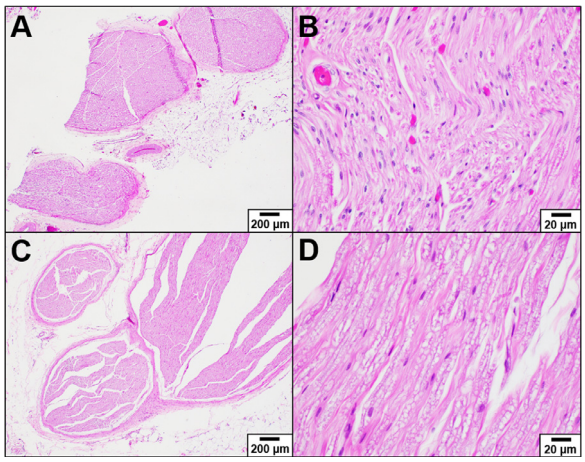

Fig. 6. A normal, healthy sciatic nerve sample was excised from amputated canine limbs and treated with histotripsy and compared against an untreated sciatic nerve sample. No histological differences were observed between the untreated samples (a: magnification 4 ×, b: magnification 40 ×) and treated samples (c: magnification 4 ×, d: magnification 40 ×).

Before resection, ultrasound imaging of the samples was performed to assess the tissue composition of the OS and to identify an optimal window for histotripsy treatment (Fig. 7a). Like the sectioned tumor samples, the two tumor samples varied in composition. The first sample was composed of primarily soft tissue tumor adjacent to lytic bone (Fig. 7a–f). The *p*- required to generate a histotripsy bubble cloud inside of the first OS tumor sample with overlying skin and muscle was measured to be 23.5 MPa. The histotripsy bubble cloud was clearly visible on ultrasound as a dense, confined hyperechoic region in the tissue, changing dynamically over time. Prefocal cavitation was occasionally observed at the skin surface in this sample, visible as oscillating hyperechoic regions at the gel–skin interface on ultrasound imaging. Compared with the first sample, the second sample had an increased amount of intact bone in the treatment path between the histotripsy transducer and the tumor. During incremental cavitation threshold testing, no visible bubble cloud was formed on ultrasound imaging for this sample because of overlying bone blockage of the OS tumor tissue. As a result, the histotripsy system was driven to its maximum voltage rating for this treatment, corresponding to a measured *p*- of 33.1 MPa. No prefocal cavitation was observed during this treatment. For both treatments, histological staining of representative tumor cells revealed variably dense regions of readily identifiable neoplastic cells (Fig. 7b, 7c). After histotripsy treatment, ablated portions of the tumor were characterized by a loss of viable tumor cells. Hemorrhage, fibrin and cellular debris replaced the ablated tumor cells (Fig. 7e, 7f). No damage to the overlying skin and muscle tissues was observed after either treatment.

DISCUSSION

This is the first study to investigate the feasibility of using histotripsy to ablate OS tumors. OS is prevalent in both humans and dogs with high mortality. Although histotripsy has been well established for the ablation of many soft tissues, histotripsy has never been investigated for the ablation of bone tumors, including OS. This study sought to determine whether histotripsy could be used to ablate primary OS by completing three experiments: (i) testing the potential of histotripsy to ablate sectioned, excised OS tumors from canine patients; (ii) testing the critical structure-sparing ability of histotripsy using healthy canine bone and nerve; and (iii) testing the potential of histotripsy to ablate excised OS tumors through intact skin/muscle layers.

The first part of this work investigated the potential of histotripsy to ablate sectioned, excised OS tumors obtained from amputated canine limbs and treated with a custom 500-kHz histotripsy transducer. OS is one of the most heterogeneous cancerous tumors in dogs and humans, with the amount of osteoid and/or bone production varying greatly between tumors and within individual tumors; chondroid and fibrous matrix may also be present (Ritter and Bielack 2010; Simpson et al. 2017). As expected, this phenomenon was observed in the excised OS samples used in this experiment. Excised samples varied in composition both within individual samples and between different samples. Some samples contained dominant regions of intact bone or mineralized tissue interspersed with small regions of lytic bone. Others were composed primarily of softer, lytic bone tissues or soft tissue tumor components and included little to no intact bone. Some samples contained regions of both types. In all samples, results indicated that histotripsy was able to achieve precise and complete ablation within the targeted volumes of the OS samples, marked by a loss of tissue architecture and cellular detail. Rare remaining cell nuclei were present in some treated tissues, but no intact tumor cells were observed in any samples after treatment. Although small fragments of ablated osteoid matrix were occasionally present after treatment, this matrix did not resemble the large, intact osteoid components present in the untreated samples. These results reveal that histotripsy not only generated complete ablation of the soft tissue components of the OS tumors but also achieved ablation of the mineralized tumor matrix (*i.e.,* osteoid matrix) of the OS tumor samples. This is a promising result for histotripsy because intact osteoid regions might otherwise serve as shielding regions for tumor cells if left untouched by histotripsy.

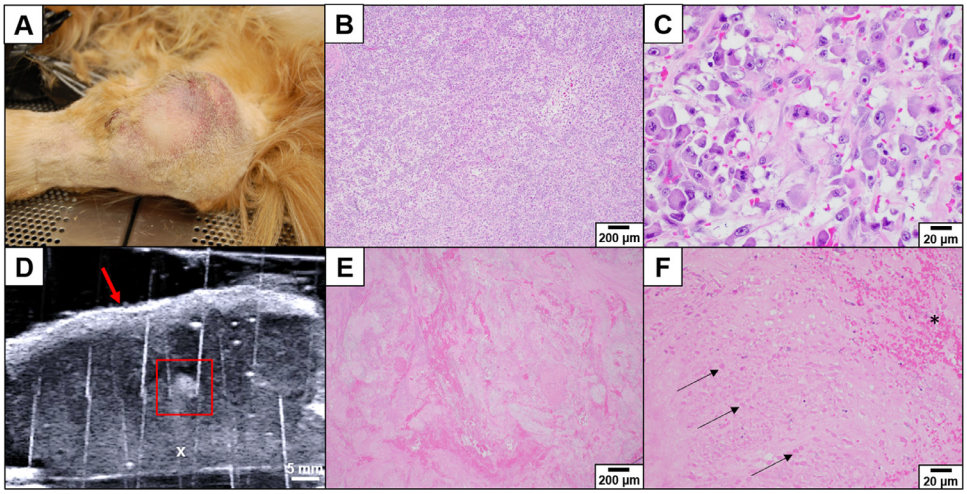

Fig. 7. Additional histotripsy treatments were completed through excised canine osteosarcoma with overlying skin and muscle tissue (a). Untreated tumor tissue contained intact cells (b: magnification 4 ×, c: magnification 40 ×) while treated tumor cells exhibited a loss of tissue architecture, non-viable cells (ghost cells, *arrows*) and hemorrhage (*asterisk*) (e: magnification 4 ×, f: magnification 40 ×). A histotripsy bubble cloud (d, *boxed*) was clearly visible throughout treatment with no loss in visibility observed because of the overlying skin and muscle layer (d, *arrow*).

The osteoid ablation observed in this study suggests that more complete ablation and better clinical results will be observed in future *in vivo* OS histotripsy treatments. Additionally, previous work has revealed that histotripsy treatments of other tumor types have resulted in rapid resorption of the treated volume by the body after treatment (Vlaisavljevich et al. 2016a, Smolock et al. 2018). As a result, we expect that the breakdown of the OS tumor tissue into tiny fragments observed here will likewise allow rapid resorption of the treated OS tissue by the body, resulting in well-tolerated OS treatments and better long-term clinical responses. Future work will investigate these phenomena *in vivo*.

The ability of histotripsy to spare critical structures near OS tissues was also tested by treating healthy canine bone and nerve samples with the same experimental histotripsy setup used for OS treatment. OS tumors develop aberrantly and often have both a bone and soft tissue component, changing the extracellular matrix composition of the affected tissues (Cui et al. 2020). As a result, OS tumors are bordered by healthy bone and muscle tissues, so histotripsy ablations of full OS tumors *in vivo* with adequate margins will require that histotripsy pulses be applied to the adjacent healthy tissues in addition to the tumor tissue. To save the affected limb while retaining its full function, these tissues should be spared or minimally damaged. In our experiments, no histological differences were observed between untreated and treated critical structure samples, suggesting that histotripsy ablation of OS may be tissue selective, with the potential to spare critical structures such as healthy bone and nerve immediately adjacent to or inside of OS tissue. This result agrees with past work indicating that histotripsy has exhibited tissue selectivity including nerve preservation in other applications (Vlaisavljevich et al. 2013). The ability of histotripsy to spare bone and nerve opens several possibilities for future OS clinical treatments. First, histotripsy may be able to generate ablation of OS tumors near critical structures without inducing damage, increasing the likelihood that the affected limb can be successfully spared with full function while complete tumor ablation is achieved. Also, histotripsy would offer a notable advantage over thermal ablation techniques, which can cause damage to peripheral bone outside of the tumor tissue. Finally, the ability of histotripsy to spare nerves may lead to a decreased risk of patients developing neuropathic pain caused by nerve trauma. Together, these possibilities warrant the future investigation of histotripsy ablation as a non-invasive, limb-sparing and tissue-selective treatment for OS tumors *in vivo*.

Together, the results of this study suggest that histotripsy is a promising technique for the treatment of primary OS in both humans and dogs. In particular, the final experiments in this study indicated the potential of histotripsy to ablate OS using a clinically relevant experimental setup to treat OS samples through intact overlying skin and muscle tissues. For both samples, histological staining of treated tissues revealed ablated portions of the tumor characterized by a loss of viable tumor cells and the presence of hemorrhage, fibrin and cellular debris. These promising results mimicked those of the sectioned OS tissues, suggesting that histotripsy is a feasible ablation technique for the treatment of OS

tumors in both veterinary and human medicine, including pediatric OS applications. Both species are currently limited to treatment options for OS involving invasive surgical intervention and chemotherapy, with metastatic disease being the primary cause of death in both species. Histotripsy offers a promising alternative to current surgical treatments, with numerous benefits and several potential applications. Unlike current standard-of-care and investigational treatments for OS, histotripsy is non-invasive and non-thermal and offers the potential to address both primary and metastatic disease. The successful ablation of excised OS samples observed in this study suggests that histotripsy may be feasible as a front-line therapy for primary OS. Surgical removal of OS tumors involves invasive procedures, whereas histotripsy offers the potential to ablate OS non-invasively with sufficient surgical margins to minimize the odds of local recurrence and development of metastatic disease without removal of large portions of bone or limb amputation. Histotripsy could also serve as a pain mitigation technique for OS, as observed for other ablation modalities (Callstrom et al. 2006; Li et al. 2009, 2010; Chen et al. 2010; Errani et al. 2011; Napoli et al. 2013; Yu et al. 2015). Recent work also suggests that histotripsy can induce immune activation toward an anti-tumor immune response (Worlikar et al., 2018; Felsted et al. 2019; Hendricks et al. 2019; Pahk et al. 2019; Worlikar et al. 2019; Eranki et al. 2020; Qu et al. 2020). Future work is planned to investigate the feasibility of ablating OS tumors with histotripsy *in vivo*, including exploration of the immunomodulatory potential of histotripsy for the treatment of OS.

Although the results of this study suggest the promise of histotripsy for the treatment of OS tumors, several possible limitations need to be investigated before clinical translation. First, the use of ultrasound imaging for histotripsy treatment monitoring may be difficult in cases where intact bone is in the treatment path. For tumors that are not amenable to ultrasound imaging, histotripsy systems guided by computed tomography or magnetic resonance imaging may be required to apply histotripsy safely and precisely, similar to systems currently being developed for transcranial histotripsy applications (Kim et al. 2014a, 2014b; Sukovich et al. 2016a, 2016b, 2020; Lu et al. 2021). OS samples with large regions of overlying intact bone may also be more difficult to treat with histotripsy for similar reasons. Encouraging results from transcranial histotripsy experiments assessing the generation of a histotripsy ablation zone through the skull have indicated that histotripsy is able to generate targeted lesions through the skull bone over a wide range of locations, with and without aberration correction (Kim et al. 2014; Sukovich et al. 2016a, 2020). These studies included work indicating histotripsy could generate lesions as close to the skull surface as 5 mm without losing treatment precision (Sukovich et al. 2016a, 2016b). This previous finding, along with the results from the current study, suggests that histotripsy will be able to generate precise ablation of OS tumors even in cases in which overlying bone is present. Finally, the safety of histotripsy for treating OS tumors will need to be investigated *in vivo* to address potential physiologic challenges such as the generation of an inflammatory response after treatment or the potential that histotripsy treatments of OS tumors could lead to increased risk of bone fracture after treatment, particularly in cases of severe tumor infiltration.

CONCLUSIONS

The results of this study illustrate the feasibility of treating OS tumors with histotripsy. Results indicate histotripsy was capable of generating complete ablation of targeted OS tumors into acellular debris using a 500-kHz transducer. In addition, healthy bone and nerve tissues were found not to be damaged using the same experimental parameters, providing initial evidence that histotripsy can be used to treat OS tumors while preserving adjacent normal tissues. Ongoing studies are underway to investigate the *in vivo* feasibility of histotripsy for treating primary canine osteosarcoma. Overall, this work suggests that histotripsy is a promising therapy for the non-invasive treatment of primary OS and should be further explored for this application.

Acknowledgments—This work was supported by grants from the American Kennel Club (Canine Health Foundation No. 02773), the Focused Ultrasound Foundation (Grant Code #453045) and the National Institute of Health (Grant Code #412613). The authors would like to thank the Virginia Tech Center for Engineered Health, the Department of Biomedical Engineering and Mechanics, and the School of Veterinary Medicine for their support of this work. The authors would also like to thank Alex Simon, Maggie Boyer, and other members of the Vlaisavljevich Research Laboratory for their assistance and support. Author Lauren Arnold was supported by the Virginia Tech ICTAS Doctoral Scholars program during the duration of this work.

Conflict of interest disclosure—L.A. has an ongoing consulting relationship with Theraclion. E.V. has an ongoing research partnership and financial relationship with HistoSonics, Inc. No other authors have a conflict of interest to report.

REFERENCES

Allen S, Hall TL, Cain C, Hernandez-Garcia L. Controlling cavitation-based image contrast in focused ultrasound histotripsy surgery. Magn Reson Med 2014;73:204–213.

Allen S, Vlaisavljevich E, Shi J, Hernandez-Garcia L, Cain C, Xu Z, Hall TL. The response of MRI contrast parameters in in vitro tissues and tissue mimicking phantoms to fractionation by histotripsy. Phys Med Biol 2017;62:7167–7180.

Bader K, Vlaisavljevich E, Maxwell A. For whom the bubble grows: Physical principles of bubble nucleation and dynamics in hisotripsy ultrasound therapy. Ultrasound Med Biol 2019;45:1056–1080.

Brodey R. The use of naturally occurring cancer in domestic animals for research into human cancer: General considerations and a review of canine skeletal osteosarcoma. Yale J Biol Med 1979;52:345–361.

Callstrom MR, Atwell TD, Charboneau JW, Farrell MA, Goetz MP, Rubin J, Sloan JA, Novotny PJ, Welch TJ, Maus TP, Wong GY, Brown KJ. Painful metastases involving bone: Percutaneous image-guided cryoablation—Prospective trial interim analysis. Radiology 2006;241:572–580.

Callstrom MR, Kurup AN. Percutaneous ablation for bone and soft tissue metastases—Why cryoablation?. Skeletal Radiol 2009;38:835–839.

Chen W, Zhu H, Zhang L, Li K, Su H, Jin C, Zhou K, Bai J, Wu F, Wang Z. Primary bone malignancy: Effective treatment with high-intensity focused ultrasound ablation. Radiology 2010;255:967–978.

Cui J, Dean D, Hornicek F, Chen Z, Duan Z. The role of extracellular matrix in osteosarcoma progression and metastasis. J Exp Clin Cancer Res 2020;39:178.

Curley SA. Radiofrequency ablation of malignant liver tumors. Oncologist 2001;6:14–23.

Ding JH, Chua TC, Glenn D, Morris DL. Feasibility of ablation as an alternative to surgical metastasectomy in patients with unresectable sarcoma pulmonary metastases. Interact Cardiovasc Thorac Surg 2009;9:1051–1053.

Edsall C, Khan Z, Mancia L, Hall S, Mustafa W, Johnsen E, Klibanov A, Durmaz Y, Vlaisavljevich E. Bubble cloud behavior and ablation capacity for histotripsy generated from intrinsic or artificial cavitation nuclei. Ultrasound Med Biol 2021;47:620–639.

Eranki A, Srinivsan P, Ries M, Kim A, Lazarski C, Rossi C, Khokhlova T, Wilson E, Knoblach S, Sharma K, Wood B, Moonen C, Sandler A, Kim P. High-intensity focused ultrasound (HIFU) triggers immune sensitization of refractory murine neuroblastoma to checkpoint inhibitor therapy. Clin Cancer Res 2020;26:1152–1161.

Errani C, Longhi A, Rossi G, Rimondi E, Biazoo A, Toscano A. Palliative therapy for osteosarcoma. Expert Rev Anticancer Ther 2011;11:217–227.

Felsted A, Qu S, Ganguly A, Pepple AL, Lee F, Xu Z, Cho C. Histotripsy ablation stimulates potentially therapeutic tumor-directed systemic immunity. Presented at the Society for Interventional Oncology Annual Meeting. Boston, MA, USA.

Fenger J, London C, Kisseberth W. Canine osteosarcoma: A naturally occurring disease to inform pediatric oncology. ILAR J 2014;55:69–85.

Friebele J, Peck J, Pan X, Abdel-Rasoul M, Osteosarcoma Mayerson J. A meta-analysis and review of the literature. Am J Orthop (Belle Mead NJ) 2015;44:547–553.

Hendricks A, Howell J, Simon A, Coutermarsh-Ott S, Allen I, Vlaisavljevich E. Investigation of the local and systemic immune response to histotripsy ablation of breast cancer in a mouse model. Presented at the meeting of the International Society for Therapeutic Ultrasound. Barcelona, Spain. June 13−15.

Jones RL, McCall J, Adam A, O'Donnell D, Ashley S, Al-Muderis O, Thway K, Fisher C, Judson IR. Radiofrequency ablation is a feasible therapeutic option in the multi modality management of sarcoma. Eur J Surg Oncol 2010;36:477–482.

Kim Y, Hall TL, Xu Z, Cain CA. Transcranial histotripsy therapy: Feasibility study. IEEE Trans Ultrason Ferroelectr Freq Control 2014a;61:582–593.

Kim Y, Owens GE, Allen SP, CA Cain, Xu Z. In vivo transcostal histotripsy therapy without aberration correction. Phys Med Biol 2014b;59:2553–2568.

Lake AM, Hall TL, Kieran K, Fowlkes JB, Cain CA, Roberts WW. Histotripsy: A minimally invasive technology for prostate tissue ablation in an in-vivo canine model. Urology 2008a;72:682–686.

Lake AM, Xu Z, Wilkinson JE, Cain CA, Roberts WW. Renal ablation by histotripsy—Does it spare the collecting system?. J Urol 2008b;179:1150–1154.

LeBlanc AK, Mazcko CN, Cherukuri A, Berger EP, Kisseberth WC, Brown ME, Lana SE, Weishaar K, Flesner BK, Bryan JN, Vail DM, Burton JH, Willcox JL, Mutsaers AJ, Woods JP, Northrup NC, Saba C, Curran KM, Leeper H, Wilson-Robles H, BG Wustefeld-Janssens, Lindley S, Smith AN, Dervisis N, Klahn S, Higginbotham ML, Wouda RM, Krick E, Mahoney JA, London CA, Barber LG, Balkman CE, McCleary-Wheeler AL, Suter SE, Martin O, Borgatti A, Burgess K, Childress MO, Fidel JL, Allstadt SD, Gustafson DL, Selmic LE, Khanna C, Fan TM. Adjuvant sirolimus does not improve outcome in pet dogs receiving standard-of-care therapy for appendicular osteosarcoma: A prospective. randomized trial of 324 dogs Clin Cancer Res 2021;27:3005.

Li C, Wu P, Liang Z, Fan W, Huang J, Zhang F. Osteosarcoma: Limb salvaging treatment by ultrasonographically guided high-intensity focused ultrasound. Cancer Biol Ther 2009;8:1102–1108.

Li C, Zhang W, Fan W, Huang J, Zhang F, Wu P. Noninvasive treatment of malignant bone tumors using high-intensity focused ultrasound. Cancer 2010;116:3934–3942.

Lin KW, Kim Y, Maxwell A, Wang TY, Hall TL, Xu Z, Fowlkes JB, Cain C. Histotripsy beyond the instrinsic cavitation threshold using very short ultrasound pulses: Microtripsy. IEEE Trans Ultrason Ferroelectr Freq Control 2014;61:251–265.

Longhi A, Errani C, De Paolis M, Mercuri M, Bacci G. Primary bone osteosarcoma in the pediatric age: State of the art. Cancer Treat Rev 2006;32:423–426.

Lu D, Raman S, Limanond P, Aziz D, Economou J, Busuttil R, Sayre J. Influence of large peritumoral vessels on outcome of radiofrequency ablation of liver tumors. J Vasc Interv Radiol 2003;14:1267–1274.

Lu N, Hall TL, Choi D, Gupta D, Daon BJ, Sukovich J, Fox A, Gerhardson T, Pandey A, Noll D, Xu Z. Transcranial MR-guided histotripsy system [e-pub ahead of print]. IEEE Trans Ultrason Ferroelectr Freq Control 2021. doi: 10.1109/TUFFC.2021.3068113.

Luetke A, Meyers P, Lewis I, Juergens H. Osteosarcoma treatment—Where do we stand? A state of the art review. Cancer Treat Rev 2014;40:523–532.

Marrero J, Pelletier S. Hepatocellular carcinoma. Clin Liver Dis 2006;10:339–351.

Meazza C, Scanagatta P. Metastatic osteosarcoma: A challenging multidisciplinary treatment. Expert Rev Anticancer Ther 2016;16:543–556.

Mitchell K, Boston S, Kung M, Dry S, Straw R, Ehrhart N, Ryan S. Outcomes of limb-sparing surgery using two generations of metal endoprosthesis in 45 dogs with distal radial osteosarcoma: A Veterinary Society of Surgical Oncology retrospective study. Vet Surg 2016;45:36–43.

Morello E, Martano M, Biology Buracco P. diagnosis and treatment of canine appendicular osteosarcoma: Similarities and differences with human osteosarcoma. Vet J 2011;189:268–277.

Napoli A, Anzidei M, Marincola B, Brachetti G, Ciolina F, Cartocci G, Marsecano C, Zaccagna F, Marchetti L, Cortesi E, Catalano C. Primary pain palliation and local tumor control in bone metastases treated with magnetic resonance-guided focused ultrasound. Invest Radiol 2013;48:351–358.

Pahk K, Shin C, Bae I, Yang Y, Kim S, Pahk K, Kim H, Oh S. Boiling histotripsy-induced partial mechanical ablation modulates tumour microenvironment by promoting immunogenic cell death of cancers. Sci Rep 2019;9:9050.

Parsons J, Cain C, Abrams G, Fowlkes J. Pulsed cavitational ultrasound therapy for controlled tissue homogenization. Ultrasound Med Biol 2005;32:115–129.

Parsons J, Cain C, Fowlkes JB. Cost-effective assembly of a basic fiber-optic hydrophone for measurement of high-amplitude therapeutic ultrasound fields. J Acoust Soc Am 2006;119:1432–1440.

Patterson E, Scudamore C, Owen D, Nagy A, Buczkowski A. Radiofrequency ablation of porcine liver in vivo: Effects of blood flow and treatment time on lesion size. Ann Surg 1998;227:559–565.

Qu S, Worlikar T, Felsted AE, Ganguly A, Beems MV, Hubbard R, Pepple AL, Kevelin AA, Garavaglia H, Dib J, Toma M, Huang H, Tsung A, Xu Z, Cho CS. Non-thermal histotripsy tumor ablation promotes abscopal immune responses that enhance cancer immunotherapy. J Immunother Cancer 2020;8:1–12.

Rho J, Ashman R, Turner C. Young's modulus of trabecular and cortical bone material: Ultrasonic and microtensile measurements. J Biomech 1993;26:111–119.

Ritter J, Osteosarcoma Bielack S. Ann Oncol 2010;21:vii320–vvii25.

Roberts W, Hall T, Ives K, Wolf JJ, Fowlkes J, Cain C. Pulsed cavitational ultrasound: A noninvasive technology for controlled tissue ablation (histotripsy) in the rabbit kidney. J Urol 2006;175:734–738.

Rowell JL, McCarthy DO, Alvarez CE. Dog models of naturally occurring cancer. Trends Mol Med 2011;17:380–388.

Simpson S, Dunning M, de Brot S, Grau-Roma L, Mongan N, Rutland C. Comparative review of human and canine osteosarcoma: Morphology, epidemiology, prognosis, treatment and genetics. Acta Vet Scand 2017;59:71.

Smolock AR, Cristescu MM, Vlaisavljevich E, Gendron-Fitzpatrick A, Green C, Cannata J, Ziemlewicz TJ, Lee FT, Jr. Robotically assisted sonic therapy as a noninvasive nonthermal ablation modality: Proof of concept in a porcine liver model. Radiology 2018;287:485–493.

Sukovich J, Xu Z, Hall TL, Allen S, Cain CA. Treatment envelope of transcranial histoptripsy applied without aberration correction. J Acoust Soc Am 2016a;140:3031.

Sukovich J, Xu Z, Kim Y, Cao H, Nguyen TS, Pandey A, Hall TL, Cain CA. Targeted lesion generation through the skull without aberration correction using histotripsy. IEEE Trans Ultrason Ferroelectr Freq Control 2016b;63:671–682.

Sukovich J, Macoskey JE, Lundt J, Gerhardson T, Hall TL, Xu Z. Real-time transcranial histotripsy treatment localization and mapping using acoustic cavitation emission feedback. IEEE Trans Ultrason Ferroelectr Freq Control 2020;67:1178–1191.

Szewcyzk M, Lechowski R, Zabielska K. What do we know about canine osteosarcoma treatment? Review. Vet Res Commun 2015;39:61–67.

Vidal Jove J, Vlaisavljevich E, Cannata J, Duryea A, Miller R, Lee F, Ziemlewicz TJ. Phase I study of safety and efficacy of hepatic histotripsy: Preliminary results of first in man experience with robotically-assisted sonic therapy. Presented at the Society for Interventional Oncology Annual Meeting. Boston, MA, USA.

Vlaisavljevich E, Kim Y, Allen S, Owens G, Pelletier S, Cain C, Ives K, Xu Z. Image-guided non-invasive ultrasound liver ablation using histotripsy: Feasibility study in an *in vivo* porcine model. Ultrasound Med Biol 2013;39:1398–1409.

Vlaisavljevich E, Kim Y, Owens G, Roberts W, Cain C, Xu Z. Effects of tissue mechanical properties on susceptibility to histotripsy-induced tissue damage. Phys Med Biol 2014a;59:253–270.

Vlaisavljevich E, Maxwell A, Warnez MT, Johnsen E, Cain C, Xu Z. Histotripsy-induced cavitation cloud initiation thresholds in tissues of different mechanical properties. IEEE Trans Ultrason Ferroelectr Freq Control 2014b;61:341–352.

Vlaisavljevich E, Lin K-W, Warnez MT, Singh R, Mancia L, Putnam AJ, Johnsen E, Cain C, Xu Z. Effects of tissue stiffness, ultrasound frequency, and pressure on histotripsy-induced cavitation bubble behavior. Phys Med Biol 2015a;60:2271–2292.

Vlaisavljevich E, Lin KW, Maxwell A, Warnez MT, Mancia L, Singh R, Putnam AJ, Fowlkes B, Johnsen E, Cain C, Xu Z. Effects of ultrasound frequency and tissue stiffness on the histotripsy intrinsic threshold for cavitation. Ultrasound Med Biol 2015b;41:1651–1667.

Vlaisavljevich E, Greve J, Cheng X, Ives K, Shi J, Jin L, Arvidson A, Hall T, Welling TH, Owens G, Roberts W, Xu Z. Non-invasive ultrasound liver ablation using histotripsy: chronic study in an in vivo rodent model. Ultrasound Med Biol 2016a;42:1890–1902.

Vlaisavljevich E, Maxwell A, Mancia L, Johnsen E, Cain C, Xu Z. Visualizing the histotripsy process: Bubble cloud−cancer cell interactions in a tissue-mimicking environment. Ultrasound Med Biol 2016b;42:2466–2477.

Vlaisavljevich E, Gerhardson T, Hall TL, Xu Z. Effects of *f*-number on the histotripsy intrinsic threshold and cavitation bubble cloud behavior. Phys Med Biol 2017a;62:1269–1290.

Wafa H, Grimer R. Surgical options and outcomes in bone sarcoma. Expert Rev Anticancer Ther 2006;6:239–248.

Ward E, Munk PL, Rashid F, Torreggiani WC. Musculoskeletal interventional radiology: Radiofrequency ablation. Radiol Clin North Am 2008;46:599–610.

Worlikar T, Vlaisavljevich E, Gerhardson T, Greve J, Wan S, Kuruvilla S, Lundt J, Ives K, Hall T, Welling TH, Lee F, Xu Z. Histotripsy for non-invasive ablation of hepatocellular carcinoma (HCC) tumor in a subcutaneous xenograft murine model. Annu Int Conf Proc IEEE Eng Med Biol Soc 2018;2018:6064–6067.

Worlikar T, Vlaisavljevich E, Gerhardson T, Greve J, Wan S, Kuruvilla S, Lundt J, Ives K, Hall TL, Welling TH, Lee F, Xu Z. Non-invasive orthotopic liver tumor ablation using histotripsy in an in vivo rodent hepatocellular carcinoma (HCC) model. Presented at. the Society for Interventional Oncology Annual Meeting. Boston, MA, USA.

Xu Z, Ludomirsky A, Eun L, Hall TL, Tran B, Fowlkes JB, Cain CA. Controlled ultrasound tissue erosion. IEEE Trans Ultrason Ferroelectr Freq Control 2004;51:726–736.

Yu W, Tang L, Lin F, Yao Y, Shen Z, Zhou X. High-intensity focused ultrasound: Noninvasive treatment for local unresectable recurrence of osteosarcoma. Surg Oncol 2015;24:9–15.

Zachos TA, Aiken SW, DiResta GR, Healey JH. Interstitial fluid pressure and blood flow in canine osteosarcoma and other tumors. Clin Orthop Relat Res 2001;385:230–236.